DETECTING STOCHASTIC NUCLEAR QUADRUPOLE RESONANCE SIGNALS IN THE PRESENCE OF STRONG RADIO FREQUENCY INTERFERENCE

S. D. Somasundaram, A. Jakobsson†, M. D. Rowe*, J. A. S. Smith*, N. R. Butt†, and K. Althoefer**

* King's College London, Division of Engineering, Strand, London, WC2R 2LS, UK
† Karlstad University, Department of Electrical Engineering, SE-651 88 Karlstad, Sweden

ABSTRACT

Nuclear quadrupole resonance (NQR) is a radio frequency (RF) spectroscopic technique, allowing the detection of many high explosives and narcotics. In practice, NQR is restricted by the low signal-to-noise ratio of the observed signals, a problem further exacerbated by the presence of strong RF interference (RFI). The current literature focuses on the use of conventional, multiple-pulsed NQR (cNQR) to obtain signals. Here, we investigate an alternative method called stochastic NQR (sNQR), having many advantages over cNQR, one of which is the availability of signal-of-interest free samples. We exploit these samples forming a matched subspace-type detector, able to efficiently reduce the influence of RFI. Further, many of the ideas already developed for cNQR, including providing robustness to uncertainties in the assumed complex amplitudes and exploiting the temperature dependencies of the NQR spectral components, are recast for sNQR. The presented detector is evaluated on both simulated and measured trinitrotoluene (TNT) data.

Index Terms— Detection, estimation, robust methods, nuclear quadrupole resonance (NQR).

1. INTRODUCTION

Nuclear quadrupole resonance (NQR) is a solid-state radio frequency (RF) technique able to detect the presence of quadrupolar nuclei, such as the ^{14}N nucleus prevalent in many explosives and narcotics [1, 2]. In conventional NQR (cNQR), multiple-pulse techniques are most often used to interrogate the sample, with powerful coherent RF modulated pulses, producing nonlinear responses. An alternative acquisition method, called stochastic NQR (sNQR), interrogates the sample using trains of low power coherent pulses, whose phases or amplitudes are randomized; herein, such pulses are termed *stochastic* pulses. Providing sufficiently weak stochastic pulses are used, the NQR system may be treated as linear and time invariant. Thus, cross-correlation of the observed time domain signal with a white input sequence yields the linear response or free induction decay (FID) which may be well modeled as a sum of exponentially damped complex sinusoids [2, 3]. In many NQR applications, RF interference (RFI) can be a major concern and in cNQR extra RFI mitigation often needs to be employed (see [2, 3] and the references therein). An important advantage of sNQR is the availability of signal-of-interest (SOI) free samples which may be exploited for interference rejection. Further advantages of sNQR, over cNQR, include lower peak RF powers, the alleviation of spin-lattice relaxation dependent delays and also the relative ease of exciting larger bandwidths [2, 4]. To increase the spectral bandwidth of the received sNQR signals, we acquire two or more data points after each stochastic pulse, as opposed to only a single point, in what is known as multiple-point acquisition (see [2, 4] for a more detailed description). The resulting correlation domain signal can then be well modeled as an FID with periodically recurring gaps. Specifically, if the sample is interrogated with a stochastic excitation sequence consisting of P stochastic pulses, and a block of N samples is acquired after each pulse, then the observed time domain signal will contain NP samples. Cross-correlation of the time domain signal with the exciting sequence, yields the correlation domain signal $r(t)$, also consisting of NP samples, which may be well modeled as a *gapped* FID, consisting of evenly spaced blocks of data, sampled at the data dwell time, D_w. The pth correlation domain block may then be written as

$$\begin{aligned} r^p(t) &= \sum_{k=1}^{d} \alpha_k \xi_k^{t+pT_s} + w(t) \quad ; \quad p = 0, \ldots, P-1 \\ \xi_k &= e^{i\omega_k(T)-\beta_k}, \end{aligned} \tag{1}$$

with $t = t_0, \ldots, t_{N-1}$, T_s, d and T denoting the block sampling time (measured with respect to the center of the stochastic pulse), the stochastic dwell time, the *known* number of FID components and the *unknown* temperature of the compound under investigation, respectively. Furthermore, α_k, $\omega_k(T)$ and β_k denote the complex amplitude, the frequency shifting function and the sinusoidal damping constant of the kth FID component, respectively. For many compounds, such as TNT, the frequency shifting functions, at likely temperatures of the compound, can be well modeled as [5]

$$\omega_k(T) = a_k - b_k T, \tag{2}$$

where a_k and b_k, for $k = 1, \ldots, d$, are given constants. Finally, $w(t)$ denotes an additive colored noise, due to thermal (Johnson) noise and external RFI, where it is here assumed that any *known* noise coloring has already been removed (c.f., [3, 6]). It is noted that the FID will have decayed to negligible levels after five times the longest spin-phase memory decay time, here denoted $T^{\star}_{2,\max}$, which can be assumed approximately known a priori. Therefore, the maximum number of correlation blocks that should be used for estimation of the FID parameters are the first $\tilde{P}$ blocks that correspond to times less than or equal to $5T^{\star}_{2,\max}$. A subset of the remaining $P - \tilde{P}$ blocks, here selected as the last $\breve{P}$ blocks, can then be used for interference and noise rejection. In this paper, we assume that the RFI lies in a low-rank linear *interference subspace* that can be estimated from the SOI-free samples. Reminiscent of the presentations in [7, 8], the interference subspace is then exploited to form a matched subspace-type detector. We term the resulting algorithm the

This work was supported, in part, by the Defence Science and Technology Laboratory (DSTL) at Fort Halstead, UK, the Swedish Research Council, Carl Trygger's Foundation, Sweden, the Swedish Foundation for International Cooperation in Research and Higher Education (STINT) and the National Science Foundation (under grant ECCS-0729727).

Corresponding author. E-mail: sdsomasundaram@hotmail.com.

SEAQUER (Subspace-based EvaluAtion of Quadrupole resonance signals Exploiting Robust methods) detector. Furthermore, similar to [3, 6], we beneficially exploit the dependencies of the NQR frequencies on temperature when forming SEAQUER. Additionally, it has been shown to be beneficial to exploit prior knowledge concerning the complex amplitudes of the NQR components [3, 6, 9]; here, we follow the approach introduced in [9], which allows such information to be exploited, but also allows for uncertainty in it.

In the following, $(\cdot)^T$, $(\cdot)^*$, $(\cdot)^\dagger$, $\|\cdot\|_2$, Re$\{\cdot\}$ and E$\{\cdot\}$ denote the transpose, the Hermitian transpose, the Moore-Penrose pseudoinverse, the two-norm, the real operator and the expectation operator, respectively.

2. THE SEAQUER ALGORITHM

Using (1), the pth data block may be expressed as

$$\mathbf{r}_N^p \triangleq \left[\begin{array}{ccc} r^p(t_0) & \ldots & r^p(t_{N-1}) \end{array} \right]^T = \mathbf{A}_{\bar{\boldsymbol{\theta}}}^p \boldsymbol{\alpha} + \mathbf{w}_N^p, \tag{3}$$

where $\mathbf{w}_N^p$ is defined similar to $\mathbf{r}_N^p$, and

$$\begin{aligned} \mathbf{A}_{\bar{\boldsymbol{\theta}}}^p &= \left[\begin{array}{ccc} \xi_1^{t_0+pT_s} & \ldots & \xi_d^{t_0+pT_s} \\ \vdots & \ddots & \vdots \\ \xi_1^{t_{N-1}+pT_s} & \ldots & \xi_d^{t_{N-1}+pT_s} \end{array} \right] \\ \boldsymbol{\alpha} &= \left[\begin{array}{ccc} \alpha_1 & \ldots & \alpha_d \end{array} \right]^T, \end{aligned} \tag{4}$$

with $\bar{\boldsymbol{\theta}} = \left[\begin{array}{cc} T & \boldsymbol{\beta}^T \end{array} \right]^T$ and $\boldsymbol{\beta} = \left[\begin{array}{ccc} \beta_1 & \ldots & \beta_d \end{array} \right]^T$ denoting the nonlinear parameter vector and the vector of unknown sinusoidal dampings, respectively. Thus, the data model for $\tilde{P}$ data blocks can be written as

$$\mathbf{r}_{N\tilde{P}} \triangleq \left[\begin{array}{ccc} (\mathbf{r}_N^0)^T & \ldots & (\mathbf{r}_N^{\tilde{P}-1})^T \end{array} \right]^T = \mathbf{H}_{\bar{\boldsymbol{\theta}}} \boldsymbol{\alpha} + \mathbf{w}_{N\tilde{P}}, \tag{5}$$

where $\mathbf{w}_{N\tilde{P}}$ is defined similar to $\mathbf{r}_{N\tilde{P}}$, and

$$\mathbf{H}_{\bar{\boldsymbol{\theta}}} = \left[\begin{array}{ccc} (\mathbf{A}_{\bar{\boldsymbol{\theta}}}^0)^T & \ldots & (\mathbf{A}_{\bar{\boldsymbol{\theta}}}^{\tilde{P}-1})^T \end{array} \right]^T. \tag{6}$$

2.1. Exploitation of the Interference Subspace

We further assume that the colored noise term, $\mathbf{w}_{N\tilde{P}}$, may be factored as

$$\mathbf{w}_{N\tilde{P}} = \mathbf{S}\boldsymbol{\phi} + \mathbf{e}_{N\tilde{P}}, \tag{7}$$

with $\mathbf{S}$, $\boldsymbol{\phi}$ and $\mathbf{e}_{N\tilde{P}}$ denoting the basis for the interference subspace, the interference subspace weights and an additive *white* Gaussian noise, respectively. Thus, (5) may be rewritten as

$$\mathbf{r}_{N\tilde{P}} = \mathbf{H}_{\bar{\boldsymbol{\theta}}} \boldsymbol{\alpha} + \mathbf{S}\boldsymbol{\phi} + \mathbf{e}_{N\tilde{P}}. \tag{8}$$

We note that the interference subspace will typically be unknown, and therefore must be estimated from the available data. Such an estimate may be formed by using the $\breve{P}$ end correlation domain data blocks, by first constructing a $N\tilde{P} \times (\breve{P}/\tilde{P})$ data matrix, $\breve{\mathbf{X}}$, in which each column consists of $\tilde{P}$ end correlation domain data blocks. Thus, $\breve{P}$ is selected as an integer multiple of $\tilde{P}$. The data matrix is then factorized using the singular value decomposition (SVD), i.e., $\breve{\mathbf{X}} = \breve{\mathbf{U}}\breve{\boldsymbol{\Sigma}}\breve{\mathbf{V}}^*$, where $\breve{\boldsymbol{\Sigma}} \in R^{N\tilde{P} \times \breve{P}/\tilde{P}}$ is a diagonal matrix with the singular values arranged in nonincreasing order on its main diagonal, and where $\breve{\mathbf{U}} \in C^{N\tilde{P} \times N\tilde{P}}$ and $\breve{\mathbf{V}} \in C^{\breve{P}/\tilde{P} \times \breve{P}/\tilde{P}}$ are unitary matrices containing the left and right singular vectors, respectively. The d_{int} dominant left singular vectors may then be used as a basis for the interference subspace $\mathbf{S} \in C^{N\tilde{P} \times d_{\text{int}}}$, i.e.,

$$\mathbf{S} = \left[\begin{array}{ccc} \breve{\mathbf{u}}_1 & \ldots & \breve{\mathbf{u}}_{d_{\text{int}}} \end{array} \right], \tag{9}$$

where $\breve{\mathbf{u}}_k$ denotes the kth left singular vector of $\breve{\mathbf{X}}$. If the interference consists of a mixture of either sinusoids or damped sinusoids, then the best choice for d_{int} is as the number of sinusoidal components. If no prior knowledge of the number of RFI components is available, then a reasonable estimate may be obtained by examining the singular values of $\breve{\mathbf{X}}$. Here, we propose using a minimum description length (MDL) like rule to select the rank of the interference subspace, forming

$$\begin{aligned} \text{MDL}(k) &= N log(\sigma_k) + (log N)k \\ d_{\text{int}} &= \arg\min_k \{\text{MDL}(k)\}, \end{aligned} \tag{10}$$

where σ_k is the kth singular value of the data matrix. We remark that a proper MDL test could also be formed, but note that the rule suggested in (10) does not require any knowledge of the probability density function and offers a fast and often adequate estimate of the model order. As is well known, the maximum likelihood estimate of $\boldsymbol{\theta} = \left[\begin{array}{ccc} \bar{\boldsymbol{\theta}}^T & \boldsymbol{\alpha}^T & \boldsymbol{\phi}^T \end{array} \right]^T$, is given by

$$\hat{\boldsymbol{\theta}} = \arg\min_{\boldsymbol{\theta}} \left\| \mathbf{H}_{\bar{\boldsymbol{\theta}}} \boldsymbol{\alpha} + \mathbf{S}\boldsymbol{\phi} - \mathbf{r}_{N\tilde{P}} \right\|_2^2. \tag{11}$$

Minimizing (11) with respect to $\boldsymbol{\phi}$ yields an estimate of $\boldsymbol{\phi}$ as

$$\hat{\boldsymbol{\phi}} = \mathbf{S}^*(\mathbf{r}_{N\tilde{P}} - \mathbf{H}_{\bar{\boldsymbol{\theta}}} \boldsymbol{\alpha}). \tag{12}$$

Substituting (12) into (11) yields the compressed minimization

$$\min_{\boldsymbol{\alpha}, \bar{\boldsymbol{\theta}}} \left\| \boldsymbol{\Pi}_{\mathbf{S}}^{\perp} \left[\mathbf{H}_{\bar{\boldsymbol{\theta}}} \boldsymbol{\alpha} - \mathbf{r}_{N\tilde{P}} \right] \right\|_2^2, \tag{13}$$

where $\boldsymbol{\Pi}_{\mathbf{S}}^{\perp} = \mathbf{I} - \mathbf{S}\mathbf{S}^*$. Thus, the data and model vectors are projected onto the space orthogonal to the interference subspace, nulling the effects of the interference.

2.2. Robust complex amplitude estimation

To exploit the prior knowledge typically available for the complex amplitudes, we follow an approach similar to the one introduced in [9], first factorizing

$$\boldsymbol{\alpha} = \rho \boldsymbol{\kappa}, \tag{14}$$

where ρ is the common (real-valued) magnitude scaling due to the signal power, and $\boldsymbol{\kappa}$ is the (complex) amplitude vector, normalized such that its largest magnitude equals unity, containing both the phases and the relative magnitudes of the d complex amplitudes. Reminiscent of [9, 10], we here consider the case when the assumed (normalized) amplitude vector, $\bar{\boldsymbol{\kappa}}$, as well as the actual (normalized) amplitude vector, $\boldsymbol{\kappa}$, belong to an uncertainty hypersphere with radius $\sqrt{\epsilon}$, i.e.,

$$\left\| \boldsymbol{\kappa} - \bar{\boldsymbol{\kappa}} \right\|_2^2 \leq \epsilon. \tag{15}$$

The choice of ϵ should reflect the uncertainty in the complex amplitudes, typically obtained as a result of the experimental setup; we refer the reader to [2, 4, 9] for further discussions on selecting ϵ. By restricting the actual (normalized) amplitude vector to this hypersphere, an estimate of the vector best fitting the observed data can be obtained by solving the following constrained minimization

$$\min_{\boldsymbol{\kappa}} \left\| \boldsymbol{\Pi}_{\mathbf{S}}^{\perp} \left[\rho \mathbf{H}_{\bar{\boldsymbol{\theta}}} \boldsymbol{\kappa} - \mathbf{r}_{N\tilde{P}} \right] \right\|_2^2 \text{ subject to } \left\| \boldsymbol{\kappa} - \bar{\boldsymbol{\kappa}} \right\|_2^2 \leq \epsilon, \tag{16}$$

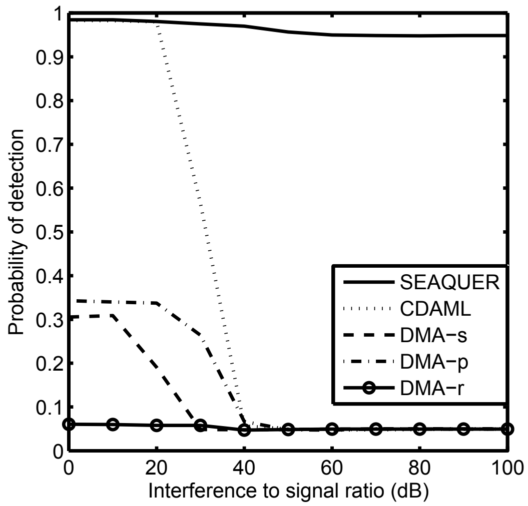

Fig. 1. The probability of detection as a function of the ISR, for $p_f = 0.05$, using simulated data with SNR $= -34$ dB.

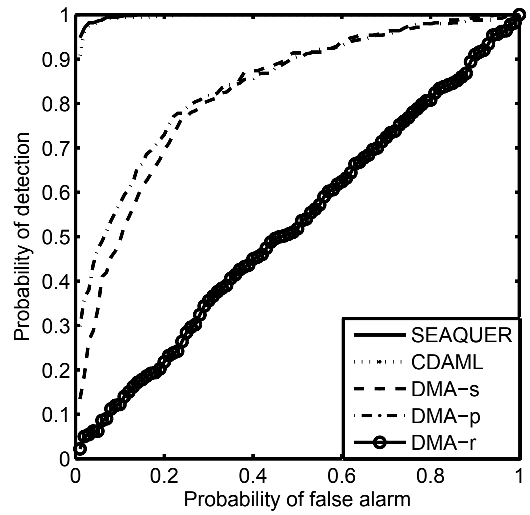

Fig. 2. The ROC curves for measured data, with (where applicable) $\epsilon = 0.1$.

where $\bar{\boldsymbol{\theta}}$ is here assumed known. It is noted that an initial estimate of ρ is needed to solve (16). By noting that ρ is the largest magnitude in $\boldsymbol{\alpha}$, an initial estimate of ρ may be obtained as

$$\hat{\rho} = \max\left\{|\hat{\boldsymbol{\alpha}}_{LS}|\right\}, \tag{17}$$

with $\max\{\mathbf{x}\}$ denoting the maximum element in the vector $\mathbf{x}$, and where

$$\hat{\boldsymbol{\alpha}}_{LS} = \left[\mathbf{H}_{\bar{\boldsymbol{\theta}}}^{*}\boldsymbol{\Pi}_{\mathbf{S}}^{\perp}\mathbf{H}_{\bar{\boldsymbol{\theta}}}\right]^{-1}\mathbf{H}_{\bar{\boldsymbol{\theta}}}^{*}\boldsymbol{\Pi}_{\mathbf{S}}^{\perp}\mathbf{r}_{N\tilde{P}} \tag{18}$$

is obtained by minimizing (13) with respect to $\boldsymbol{\alpha}$. Using the SVD to factor $\boldsymbol{\Pi}_{\mathbf{S}}^{\perp}\mathbf{H}_{\bar{\boldsymbol{\theta}}} = \mathbf{U}\boldsymbol{\Sigma}\mathbf{V}^{*}$, the minimization in (16) can be rewritten as

$$\min_{\tilde{\boldsymbol{\kappa}}}\left\|\rho\boldsymbol{\Sigma}\tilde{\boldsymbol{\kappa}} - \tilde{\mathbf{r}}\right\|_2^2 \text{ subject to } \left\|\mathbf{V}[\boldsymbol{\kappa} - \tilde{\bar{\boldsymbol{\kappa}}}]\right\|_2^2 \leq \epsilon, \tag{19}$$

where $\tilde{\mathbf{r}} = \mathbf{U}^{*}\boldsymbol{\Pi}_{\mathbf{S}}^{\perp}\mathbf{r}_{N\tilde{P}}$, $\tilde{\boldsymbol{\kappa}} = \mathbf{V}^{*}\boldsymbol{\kappa}$ and $\tilde{\bar{\boldsymbol{\kappa}}} = \mathbf{V}^{*}\bar{\boldsymbol{\kappa}}$. If the unconstrained least squares solution of $\tilde{\boldsymbol{\kappa}}$ is within the feasible region then it is a solution to (19); however, if this is not the case then the solution will occur on the boundary of the feasible region and is found from

$$\min_{\tilde{\boldsymbol{\kappa}}}\left\|\rho\boldsymbol{\Sigma}\tilde{\boldsymbol{\kappa}} - \tilde{\mathbf{r}}\right\|_2^2 \text{ subject to } \left\|\mathbf{V}[\boldsymbol{\kappa} - \tilde{\bar{\boldsymbol{\kappa}}}]\right\|_2^2 = \epsilon, \tag{20}$$

which can be solved using the method of Lagrange multipliers. In the interest of brevity, we refer the reader to [2, 9] for further details on finding the $\tilde{\boldsymbol{\kappa}}$ satisfying (19). To ensure that ρ and $\boldsymbol{\kappa}$ are uniquely defined, the robust estimate of $\boldsymbol{\kappa}$ is formed as

$$\hat{\boldsymbol{\kappa}} = \frac{\mathbf{V}\tilde{\boldsymbol{\kappa}}}{\max\{|\mathbf{V}\tilde{\boldsymbol{\kappa}}|\}}. \tag{21}$$

Given $\hat{\boldsymbol{\kappa}}$, ρ may be reestimated as

$$\hat{\hat{\rho}} = \text{Re}\{(\boldsymbol{\Pi}_{\mathbf{S}}^{\perp}\mathbf{H}_{\bar{\boldsymbol{\theta}}}\hat{\boldsymbol{\kappa}})^{\dagger}\mathbf{r}_{N\tilde{P}}\}. \tag{22}$$

Forming

$$\hat{\boldsymbol{\alpha}} = \hat{\boldsymbol{\kappa}}\hat{\hat{\rho}}, \tag{23}$$

and substituting it into (13) yields the residual least squares error

$$\varphi_{\bar{\boldsymbol{\theta}}} = \left\|\boldsymbol{\Pi}_{\mathbf{S}}^{\perp}(\mathbf{H}_{\bar{\boldsymbol{\theta}}}\hat{\boldsymbol{\alpha}}_{\bar{\boldsymbol{\theta}}} - \mathbf{r}_{N\tilde{P}})\right\|_2^2, \tag{24}$$

between the model and the observed data, where we have used the notation $\hat{\boldsymbol{\alpha}}_{\bar{\boldsymbol{\theta}}}$ to stress the dependence of $\hat{\boldsymbol{\alpha}}$ on $\bar{\boldsymbol{\theta}}$. In general, the nonlinear parameter vector, $\bar{\boldsymbol{\theta}}$, will be unknown and must be estimated by minimizing $\varphi_{\bar{\boldsymbol{\theta}}}$ over $\bar{\boldsymbol{\theta}}$, using a grid search. Thus, for each value of $\bar{\boldsymbol{\theta}}$, the residual error, $\varphi_{\bar{\boldsymbol{\theta}}}$, is evaluated using (16)–(24). The estimated value of $\bar{\boldsymbol{\theta}}$ is then found as the parameter vector minimizing this error, i.e.,

$$\hat{\bar{\boldsymbol{\theta}}} = \arg\min_{\bar{\boldsymbol{\theta}}} \varphi_{\bar{\boldsymbol{\theta}}}. \tag{25}$$

The test statistic is formed as an (approximate) generalized likelihood ratio (GLRT) detector, i.e.,

$$T(\mathbf{r}_{N\tilde{P}}, \hat{\boldsymbol{\alpha}}_{\hat{\bar{\boldsymbol{\theta}}}}) = \frac{\mathbf{r}_{N\tilde{P}}^{*}\boldsymbol{\Pi}_{\mathbf{S}}^{\perp}\mathbf{r}_{N\tilde{P}}}{\left\|\boldsymbol{\Pi}_{\mathbf{S}}^{\perp}(\mathbf{r}_{N\tilde{P}} - \mathbf{H}_{\hat{\bar{\boldsymbol{\theta}}}}\hat{\boldsymbol{\alpha}}_{\hat{\bar{\boldsymbol{\theta}}}})\right\|_2^2}, \tag{26}$$

where the signal component is deemed present iff $T(\mathbf{r}_{N\tilde{P}}, \hat{\boldsymbol{\alpha}}_{\hat{\bar{\boldsymbol{\theta}}}}) > \gamma$, and otherwise not, where γ is a predetermined threshold value reflecting the acceptable probability of false alarm (p_f). We remark that the so-obtained SEAQUER detector requires a $(d+1)$-dimensional search over the nonlinear parameter space. As noted in [3, 6, 9], this full search may be well approximated using $(d+1)$ one-dimensional searches, which may be iterated to further improve the fitting. We are currently working on deriving the distribution of the detector, under the null hypothesis, in closed form as a function of ϵ and the search space. Therefore, for now, we resort to Monte Carlo evaluation. Numerical examples in [4] illustrate that when RFI is absent, the detector has a constant false alarm rate (CFAR) with respect to the unknown noise variance. When RFI is present, the detector is approximately CFAR with respect to the unknown RFI subspace and its power.

3. NUMERICAL EXAMPLES

In this section, we examine the performance of the proposed detectors using both simulated and measured sNQR data. The measured data consisted of 1000 data files, 500 with TNT present and 500 without, each taking 30 seconds to acquire. The sample, consisting of 180 g creamed monoclinic TNT, was placed inside a shielded

Table 1. Estimates of sNQR signal parameters for the $d = 5$ v_+ lines of monoclinic TNT, for an excitation frequency of 843 kHz, in the region of 830-860 kHz.

k	1	2	3	4	5
ω_k	1.9567	0.6214	0.1183	-0.0724	-0.7690
β_k	0.0401	0.0128	0.0122	0.0192	0.0207
$\lvert\kappa_k\rvert$	0.46	0.25	0.56	1.00	0.80
$\angle\kappa_k$ (rads)	-0.1664	2.5218	-2.7135	-2.2918	-0.7020

solenoidal coil and maintained at a temperature of 295.15–296.15 K. A length $P = 511$ stochastic excitation sequence was used, in which the phases of the RF pulses were randomized with either 0 or $180°$ phase shifts, using a maximum length binary sequence (MLBS). For each 30 s data file, this sequence was repeatedly applied, and the responses from each sequence summed up. Following each stochastic pulse, $N = 64$ data points were acquired, where $D_w = 2 \times 10^{-5}$s, yielding a time domain sequence consisting of $NP = 32704$ samples. This time-domain signal was then cross-correlated using the fast Hadamard transform to obtain the correlation domain signal. Table 1 summarizes the sNQR signal parameters, estimated from a high SNR signal, obtained by summing around 8 hours of data. The detectors were also compared on simulated data, designed to mimic the measured data, which was generated using (1), (2) together with the temperature shifting function constants for monoclinic TNT (see, e.g., [5, 6]), and Table 1. RFI components were added to the *time-domain* sNQR signal, i.e., before cross-correlation. Similar to the RFI model used in [3], the RFI is modeled as a set of discrete sinusoids whose frequencies and phases are uniformly distributed (over the interval $[-\pi, \pi]$), and with randomly distributed magnitudes; here, we used six discrete sinusoids. The interference-to-(noise-free) NQR signal ratio (ISR) is here defined as ISR $= \sigma_I^2 \sigma_s^{-2}$, where σ_I^2 and σ_s^2 denote the power of the interference and the noise-free signal, respectively. Furthermore, we define SNR $= \sigma_s^2 \sigma_e^{-2}$, where σ_e^2 and σ_s^2 denote the power of the high-rank (Johnson) noise and the power of the noise-free signal, respectively. In the examples using simulated data, the results were obtained from 1500 Monte-Carlo simulations. Here, we will examine the interference rejection capabilities of the algorithms. As a reference, we will also compare the presented detector to the correlation domain approximate maximum likelihood detector (CDAML) and the demodulation approaches (DMA) [2, 3, 6, 11]. From Table 1, we note that $5T^{\star}_{2,\text{max}}$ corresponds to around 410 normalized samples; therefore, we have chosen $\tilde{P} = 5$. Furthermore, we have selected $\breve{P} = 320$. The SEAQUER, CDAML and DMA-s detectors use a search region over temperature of [290, 300] K (in 100 steps). Furthermore, the SEAQUER and CDAML detectors use a search over each of the d sinusoidal dampings of $\beta_k = [0.01, 0.05]$ (in 100 steps). Figure 1 illustrates the probability of detection (p_d) as a function of the ISR, for simulated data with RFI, where the uncertainty in the complex amplitudes is selected as zero and therefore $\epsilon = 0$. The figure illustrates the benefits of the proposed SEAQUER algorithm, especially for ISR ≥ 30 dB, where the effect of increasing the ISR on p_d is negligible. It is noted that for low ISR, the SEAQUER detector performs similarly to the CDAML detector, but with increasing ISR, the performances of the CDAML and DMA-based detectors deteriorate rapidly, as they have no means with which to counter the strong RFI. As detection is the problem of interest, we finally proceed to examine the receiver operating characteristic (ROC) curves for the SEAQUER, CDAML and DMA-detectors, using real data. Figure 2 illustrates these ROC curves, indicating that there is a distinct gain for the proposed detector even when there is no RFI present in the data. We remark that the SEAQUER detector, unlike the CDAML and DMA approaches, is robust to uncertainties in the assumed normalized complex amplitudes.

4. REFERENCES

[1] A. N. Garroway, M. L. Buess, J. B. Miller, B. H. Suits, A. D. Hibbs, A. G. Barrall, R. Matthews, and L. J. Burnett, "Remote Sensing by Nuclear Quadrupole Resonance," *IEEE Trans. Geoscience and Remote Sensing*, vol. 39, no. 6, pp. 1108–1118, June 2001.

[2] S. D. Somasundaram, *Advanced Signal Processing Algorithms Based on Novel Nuclear Quadrupole Resonance Models for the Detection of Explosives*, Ph.D. thesis, King's College London, London, United Kingdom, 2007.

[3] S. D. Somasundaram, A. Jakobsson, J. A. S. Smith, and K. Althoefer, "Exploiting Spin Echo Decay in the Detection of Nuclear Quadrupole Resonance Signals," *IEEE Trans. Geoscience and Remote Sensing*, vol. 45, no. 4, pp. 925–933, April 2007.

[4] S. D. Somasundaram, A. Jakobsson, M. D. Rowe, J. A. S. Smith, N. R. Butt, and K. Althoefer, "Robust Detection of Stochastic Nuclear Quadrupole Resonance Signals," Submitted to *IEEE Trans. Signal Processing*.

[5] J. A. S. Smith, M. D. Rowe, R. M. Deas, and M. J. Gaskell, "Nuclear Quadrupole Resonance Detection of Landmines," in *Conference Requirements and Technologies for the Detection, Removal and Neutralization of Landmines and UXO*, September 2003, vol. 2, pp. 715–721.

[6] A. Jakobsson, M. Mossberg, M. D. Rowe, and J. A. S. Smith, "Exploiting Temperature Dependency in the Detection of NQR Signals," *IEEE Trans. Signal Processing*, vol. 54, no. 5, pp. 1610–1616, May 2006.

[7] R. T. Behrens and L. L. Scharf, "Signal Processing Applications of Oblique Projection Operators," *IEEE Transactions on Signal Processing*, vol. 42, no. 6, pp. 1413–1424, June 1994.

[8] L. L. Scharf and B. Friedlander, "Matched Subspace Detectors," *IEEE Transactions on Signal Processing*, vol. 42, no. 8, pp. 2146–2157, August 1994.

[9] S. D. Somasundaram, A. Jakobsson, and E. Gudmundson, "Robust Nuclear Quadrupole Resonance Signal Detection Allowing for Amplitude Uncertainties," To appear in *IEEE Trans. Signal Processing*.

[10] J. Li, P. Stoica, and Z. Wang, "On Robust Capon Beamforming and Diagonal Loading," *IEEE Transactions on Signal Processing*, vol. 51, no. 7, pp. 1702–1715, July 2003.

[11] S. D. Somasundaram, A. Jakobsson, N. R. Butt, M. D. Rowe, J. A. S. Smith, and K. Althoefer, "Detection of Stochastic Nuclear Quadrupole Resonance Signals," in *15th IEEE International Conference on Digital Signal Processing*, Cardiff, UK, July 2007, pp. 367–370.